LETTER

Intersplat Friction Force and Splat Sliding in a Plasma-Sprayed Aluminum Alloy Coating during Nanoindentation and Microindentation

Yao Chen, Srinivasa Rao Bakshi, and Arvind Agarwal*

Department of Mechanical and Materials Engineering, Florida International University, 10555 West Flagler Street, Miami, Florida 33174

ABSTRACT This study computes the friction force during splat sliding in the plasma-sprayed Al−Si coating based on the instrumented depth-sensing nanoindentation and microindentation experiments. A small intersplat friction force ($\sim 10^{-4}$ N) contributes to the occurrence of the splat sliding. As compared with nanoindentation, more and more splat sliding occurs during microindentation because of the increase in the applied load, which accounts for the ~26% loss of the elastic modulus.

KEYWORDS: internal friction • indentation • coating • plasma deposition

1. INTRODUCTION

The plasma spray technique is a versatile process that can deposit a wide range of alloys, ceramics, polymers, and composites as coatings while retaining the benefits of rapid solidification (1). Plasma-sprayed coatings are formed by the stacking of thin splats, which are produced by a stream of molten and semimolten droplets impacting on the substrate followed by flattening and rapid solidification. The typical microstructure of the plasma-sprayed deposit consists of layered splat structures, intersplat pores, microcracks, and fine voids, which often lead to inadequate bond strength between the splats (2). Previous investigations revealed that the elastic moduli of plasma-sprayed coatings are much lower than those of bulk, dense materials (3−9). For example, the elastic modulus (evaluated using the bending test) of an atmosphere plasma-sprayed yttria-stabilized zirconia (YSZ) top coating with ~15% porosity is only 1−2% of that for dense YSZ (4). The elastic modulus of a plasma-sprayed NiCrAlY coating measured by spherical microindentation decreases to 80 ± 12 GPa (8), as compared to 200 GPa for dense NiCrAlY. The relationship between the elastic modulus and porosity, often used in the evaluation of the elastic moduli of porous materials, is (10)

$$E = E_0 \exp(-b_e P) \quad (1)$$

in which b_e is a constant (~2), E_0 the elastic modulus of a dense material, and P the porosity. However, the calculated elastic moduli of plasma-sprayed coatings using eq 1 are much higher than the experimentally measured values (4, 8). The unsatisfactory prediction of the elastic modulus from eq 1 strongly implies that the porosity is not the sole factor in determining the elastic modulus. Consequently, some researchers proposed that the significant decrease in the elastic modulus of a plasma-sprayed coating is ascribed to splat sliding (4) and/or a low effective bonding ratio (5, 6). The bonding ratio is defined as the ratio of the total bonded lamellar interface areas to the total apparent interface areas between flattened splats (5, 6). It should be noted that the intrinsic inhomogeneous microstructure of the as-sprayed coating always leads to anisotropic elastic moduli along the cross-sectional and axial directions of the deposit. Nevertheless, the splat sliding can be activated if the external load is applied along either the cross-sectional or axial direction because of the lower bonding ratio between adjacent splats. However, it has been an unresolved issue for years to estimate the intersplat friction force for splat sliding. In the present study, nanoindentation and microindentation experiments were conducted on the plasma-sprayed Al−Si coating, and the intersplat friction force for splat sliding was estimated using an analytical model.

2. EXPERIMENTAL PROCEDURES

Gas-atomized, prealloyed, spherical Al−11.6 wt % Si alloy (referred to as Al−Si hereafter) powder with a size of 14 ± 9 μm was selected as the precursor powder. Plasma spray was carried out using a SG-100 gun (Praxair, Inc., Danbury, CT), with processing parameters as follows: 40 V; current of 550 A, primary gas argon (42.5 slm), secondary gas helium (30.5 slm), carrier gas argon (11.9 slm), standoff distance of 100 mm, and powder feed rate of 20 g/min. The porosity of the plasma-sprayed coating was estimated by image analysis. To guarantee the measured porosity of the as-sprayed coating, the average of the porosity was calculated based on the image analysis results for five different regions of the as-sprayed coating. Nanoindentation tests were carried out using Hysitron Triboindenter (Hysitron, Minneapolis, MN) with a diamond Berkovich tip. During nanoindentation, the load was applied at the rate of 25 μN/s up to a peak load of 2300 μN, where it was held for 2 s and then unloaded completely at a negative rate of 25 μN/s.

* Corresponding author. Phone: 305-348-1701. Fax: 305-348-1932. E-mail: agarwala@fiu.edu.
Received for review October 12, 2008 and accepted November 14, 2008

DOI: 10.1021/am800114h

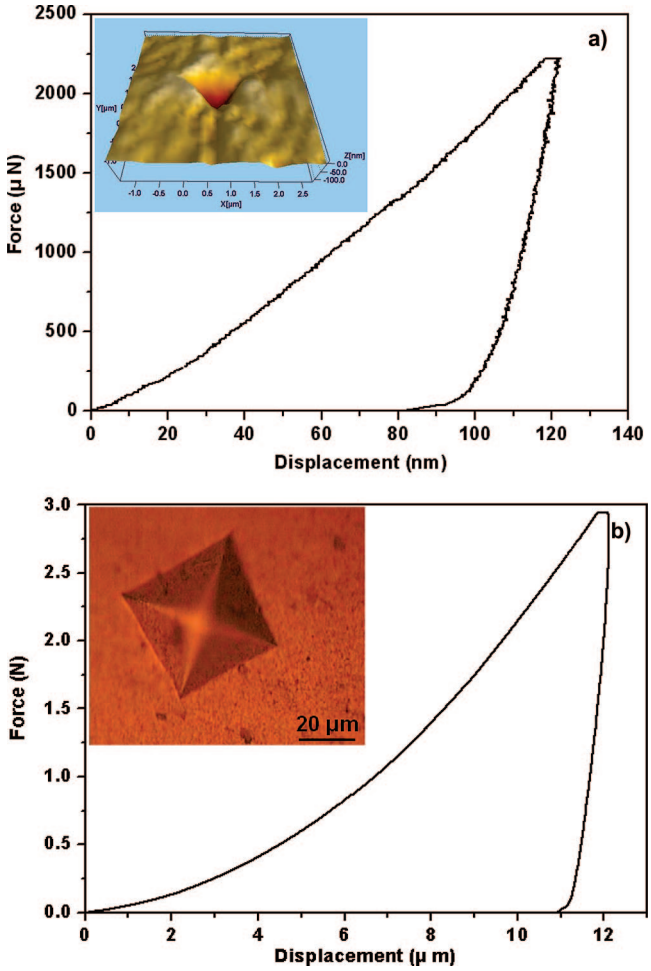

FIGURE 1. Load−displacement curve from (a) nanoindentation and a scanning probe microscope image of the indent and (b) microindentation and an optical micrograph of the indent (all indentations were made on a cross section of the plasma-sprayed Al−Si coating).

Additionally, continuous load/displacement measurements with a Vickers microindenter were also conducted on a polished cross section of the Al−Si sample using a depth-sensing indentation instrument (MHT, Micro Photonics Inc., Allentown, PA), in which the load was applied at the rate of 1633 μN/s up to a peak load of 2.94 N, where it was held for 15 s and then unloaded completely at a rate of 1633 μN/s. The hardness and elastic modulus were estimated by the Oliver and Pharr method (11). It is noted that all of the nanoindentation and microindentation were made on a polished cross section of the plasma-sprayed Al−Si coating.

3. RESULTS AND DISCUSSION

Representative load−displacement curves of nanoindentation and microindentation made on a cross section of the Al−Si coating (average thickness ~550 μm) are shown in Figure 1. It is seen that the loading−unloading curves of nanoindentation are serrated, which is attributed to its finely distributed porosity (~5.3 vol %) throughout the plasma-sprayed coating. Comparatively, the loading−unloading curves of microindentation are smooth, indicating that a Vickers tip with a larger size is insensitive to these fine pores and microcracks within the coating. The elastic modulus and hardness of the plasma-sprayed Al−Si coating, measured by nanoindentation, are 112 ± 9.4 and 1.1 ± 0.2 GPa, respectively. Vickers microindentation results show that the Al−Si coating exhibits an elastic modulus of 83.6 ± 5.7 GPa and a hardness of 0.88 ± 0.06 GPa.

The Vickers hardness is ~80% of the nanohardness because nanoindentation analysis utilizes the projected contact area at the peak load instead of the residual projected area. Also, it assumes a pure elastic contact describing the elastic/plastic indentation process (12).

The elastic modulus of the plasma-sprayed Al−Si coating measured by microindentation is ~74% of that measured by nanoindentation. This is attributed to the large difference in the scale length of the elastoplastic deformation region produced by the Berkovich and Vickers tips, respectively. The radius (c) of the elastoplastic deformation region beneath the Berkovich or Vickers tip can be estimated using eqs 2 (13) and 3 (14), respectively

$$c = \sqrt{\frac{0.3F_{max}}{\sigma_y}} \tag{2}$$

$$c = \sqrt{\frac{0.48F_{max}}{\sigma_y}} \tag{3}$$

where F_{max} is the maximum normal force applied on the indent tip and $\sigma_y$the yield strength of the tested sample.

The yield strength during microindentation is estimated based on the relationship between the yield strength (σ_y), and the Vickers hardness (H_V) obeys (15)

$$\sigma_y\,(\mathrm{MPa}) = 3.55H_V\,(\mathrm{kg/mm^2}) \tag{4}$$

The computed yield strength of the plasma-sprayed Al−Si coating from the Vickers hardness is 294.5 ± 21.4 MPa. Assuming that the as-sprayed coating is an elastic-perfectly plastic material, the relationship between the nanohardness and yield strength is $H/\delta_y = 3$ (13). Hence, the computed yield strength of the as-sprayed Al−Si coating is ~366.7 ± 66.6 MPa from the nanohardness. The computed yield strength is substituted in eqs 2 and 3 to obtain the size of the elastoplastic region for nanoindentation and microindentation, respectively. The radius of the elastoplatic region is 1.39 ± 0.13 μm for nanoindentation and 69.5 ± 2.5 μm for microindentation. Figure 2 shows that the splat morphology is disklike with a radius of 65 ± 20 μm and a thickness of ~1−1.5 μm. It can be concluded that the elastoplastic deformation region caused by the Berkovich tip contains only 2−3 splats, whereas the elastoplastic deformation region beneath the Vickers tip contains as many as 90−142 splats. Thereby, it is argued that the lower elastic modulus of the plasma-sprayed coating based on Vickers microindentation is due to the splat sliding and entrapped porosity between splats.

The identification of the stress−strain parameters while a sharp tip was pressed into a material was derived by Tabor (16) as

$$\sigma = \frac{F_{max}}{AM} \tag{5}$$

where F_{max} is the maximum applied normal force, A the contact area of a sharp tip pressed into a material, and M

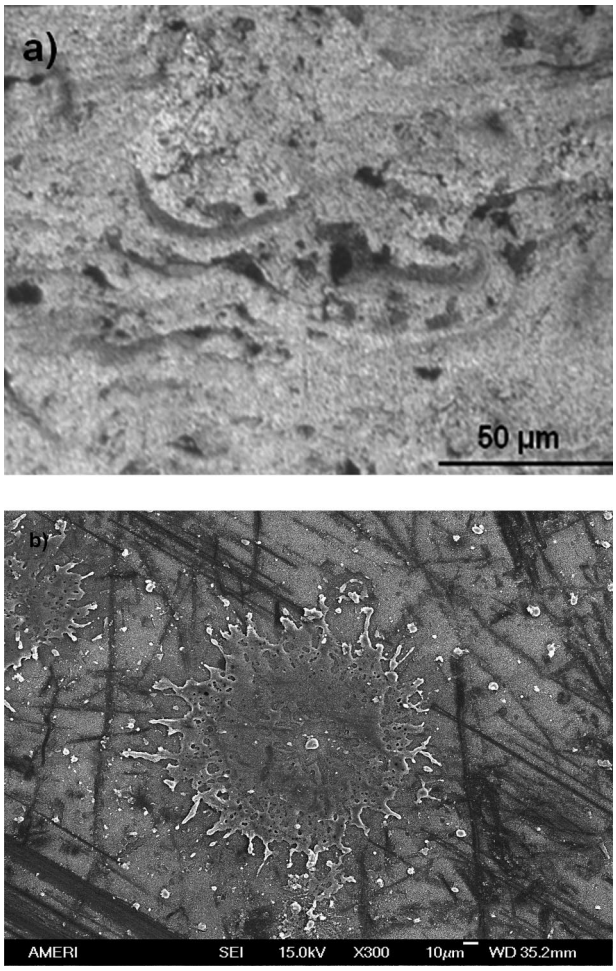

FIGURE 2. (a) Optical micrograph of the cross section of the plasma-sprayed Al–Si coating and (b) SEM image showing single-splat morphology.

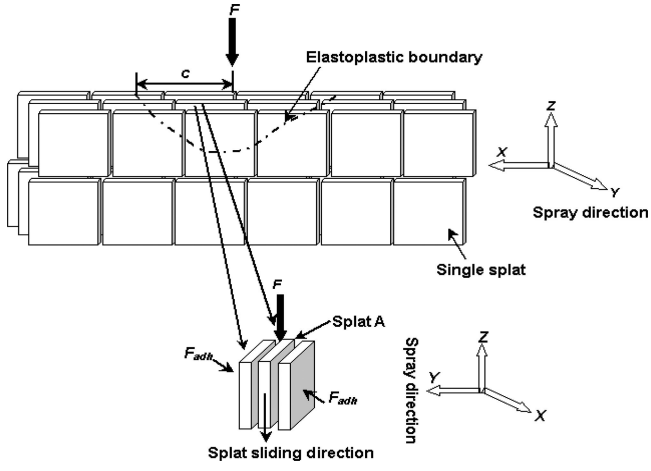

FIGURE 3. Schematic illustration of splat sliding as a consequence of the load applied through a sharp tip on a cross section of the plasma-sprayed coating.

the constant with a value of 2.9 in Tabor's original approach (16).

Figure 3 shows that sliding of splat A occurs under an applied normal force. The friction force will be produced because of the existence of an adhesion force between splat A and neighboring splats, as shown in Figure 3, which is viewed from the *X* direction. It is noted that the adhesion force (F_{adh}) between splat A and neighboring splats is compressive in nature and is applied on splat A. Considering the friction force caused by splat sliding within the elastoplastic deformation region, the stress (σ) on the splat can be developed as

$$\sigma = \frac{F_{max} - 2\mu F_{adh} N}{AM} \tag{6}$$

in which F_{adh} is the adhesion force between splats, μ the coefficient of friction between splats, and N the splat number included within the elastoplastic deformation region.

To compute the intersplat friction force (μF_{adh}), the contact area produced by the Berkovich and Vickers tips should be known, respectively. It is well-known that the maximum displacement (h_m) at the peak load equals the sum of the contact depth (h_c) and the elastic surface displacement at the perimeter of the contact (h_s) (17), i.e.,

$$h_m = h_c + h_s \tag{7}$$

Bao et al. (18) defined recovery resistance (R_s) as a material property to be an indicator of energy dissipation during an indentation cycle

$$R_s = \frac{F_{max}}{h_s^2} = 2.263\frac{E_r^2}{H} \tag{8}$$

where E_r and H are the reduced elastic modulus and the hardness by nanoindentation experiments. Then, the contact area in the process of nanoindentation is estimated using (14)

$$A \approx 24.5 h_c^2 \tag{9}$$

Therefore, the contact area is estimated to be approximately 0.31 μm^2. Comparatively, the true contact area (A_{true}) in the process of microindentation can be expressed as (14)

$$A_{true} = \frac{F_{max}}{H} \tag{10}$$

where H is the Vickers hardness. Subsequently, the contact area for microindentation ranges from 3000 to 3600 μm^2.

On the basis of the assumption of *uniformity of the adhesive force along the splat interface and neglect of voids at the splat interface*, by substitution of the estimated yield strength, contact area, and number of splats included within the elastoplastic deformation region for both indentation techniques in eq 5, the friction force during splat sliding in nanoindentation and microindentation can be obtained as eqs 11 and 12, respectively,

$$\mu F_{adh} = F_f = (511 \pm 2) \times 10^{-6}\ \text{N} \tag{11}$$

$$\mu F_{adh} = F_f = (493 \pm 176) \times 10^{-6}\ \text{N} \tag{12}$$

where F_f is the friction force of splat sliding.

It is evident from eqs 11 and 12 that the computed friction force (μF_{adh}) during splat sliding is almost the same (the difference comes from the model error) for nanoindentation and microindentation, strongly implying that the friction force (μF_{adh}) between splats is an intrinsic mechanical property for a given plasma-sprayed coating. Meanwhile, such a small friction force ($\sim 10^{-4}$ N) indicates that splat

sliding can be easily activated. It is also evident that the total number of splats included within the elastoplastic deformation region beneath the sharp indenter tip increases with an increase in the applied load. Subsequently, more and more splat sliding can be activated, leading to a significant loss of the measured elastic modulus. Similar analytical models could be developed for other plasma-sprayed coatings provided it takes into account the dependence on the real splat contact area and intersplat porosity, which is a function of the processing parameters.

4. CONCLUSIONS

In summary, the plasma-sprayed Al−Si coating shows that the measured elastic modulus by microindentation is only ∼74% of that from nanoindentation. The computed friction force between splats is $\sim 10^{-4}$ N for the plasma-sprayed Al−Si coating. The intersplat friction force is an intrinsic property of the coating and independent upon the applied load during indentation tests. An increase in the applied indentation load causes a higher degree of splat sliding, which contributes to a loss of the elastic modulus.

Acknowledgment. The authors acknowledge funding from the National Science Foundation CAREER Award (NSF-DMI-0547178) and the DURIP (Grant N00014-06-0675) grant from the Office of Naval Research.

REFERENCES AND NOTES

(1) Fauchais, P. *J. Phys. D* **2004**, *37*, R86–R108.
(2) Fauchais, P.; Fukumoto, M.; Vardelle, A.; Vardelle, M. *J. Therm. Spray Technol.* **2004**, *13*, 337–360.
(3) Leigh, S. H.; Lin, C. K.; Berndt, C. C. *J. Am. Ceram. Soc.* **1997**, *80*, 2093–2099.
(4) Tang, F.; Schoenung, J. M. *Scr. Mater.* **2006**, *54*, 1587–1592.
(5) Li, C. J.; Ohmori, A.; Mcpherson, R. *J. Mater. Sci.* **1997**, *32*, 997–1004.
(6) Li, C. J.; Ohmori, A. *J. Therm. Spray Technol.* **2002**, *11*, 365–374.
(7) Zhao, J.; Silberschnidt, V. V. *Mater. Sci. Eng. A* **2006**, *417*, 287–293.
(8) Alcalá, J.; Gaudette, F.; Suresh, S.; Sampath, S. *Mater. Sci. Eng. A* **2001**, *316*, 1–10.
(9) Kim, H.-J.; Kweon, Y. G. *Thin Solid Film* **1999**, *342*, 201–206.
(10) Spriggs, R. M. *J. Am. Ceram. Soc.* **1961**, *44*, 628–629.
(11) Pharr, G. M.; Oliver, W. C.; Brotzen, F. R. *J. Mater. Res.* **1992**, *7*, 613–617.
(12) Qian, L. M.; Li, M.; Zhou, Z. R.; Yang, H; Shi, X. Y. *Surf. Coat. Technol.* **2005**, *95*, 264–271.
(13) Giannakopoulos, A. E.; Suresh, S. *Scr. Mater.* **1999**, *40*, 1191–1198.
(14) Zeng, K.; Söderlund, E.; Giannakopoulos, A. E.; Rowcliffe, D. G. *Acta Mater.* **1996**, *44*, 1127–1141.
(15) Busby, J. T.; Hash, M. C.; Was, G. S. *J. Nucl. Mater.* **2005**, *336*, 267–278.
(16) Tabor, D. *The Hardness of Metal*; Clarendon Press: Oxford, U.K., 1951; p 175.
(17) Oliver, W. C.; Pharr, G. M. *J. Mater. Res.* **1992**, *7*, 1564–1583.
(18) Bao, Y. W.; Wang, W.; Zhou, Y. C. *Acta Mater.* **2004**, *52*, 5397–5404.

AM800114H